Physics and Chemistry of Minerals (2025) 52:32
https://doi.org/10.1007/s00269-025-01333-9

ORIGINAL PAPER

The impact of local ordering on physical properties in Fe-Mg solid solutions

Christin Wiggers[1,2] · **Ella M. Schmidt**[1,2,3]

Received: 24 June 2025 / Accepted: 2 October 2025 / Published online: 4 November 2025

Abstract

We investigate the influence of short-range Mg–Fe cation ordering on the elastic and vibrational properties of olivine $(Fe_{xx}Mg_{1-x})_2SiO_4$ $(0<x<1)$ and ferropericlase $(Fe_{xx}Mg_{1-x})O$ $(0<x<1)$ solid solutions using atomistic simulations based on empirical force fields. Supercells representing distinct local distributions of Mg and Fe cations around equiatomic composition (Fe:Mg 50:50, x 0.5) were generated and structurally relaxed. Short range order states include cation clustering, random cation ordering and preferred heteroatom paring. In both solid solution series, bulk physical properties, such as elastic moduli and seismic velocities, are primarily controlled by overall composition rather than the specific local cation arrangement. However, vibrational properties such as heat capacity and the phonon dispersion curves reveal a stronger sensitivity to short-range order. This sensitivity is enhanced in structurally simpler ferropericlase, while the increased structural complexity of olivine suppresses these differences.

Keywords Local order · Olivine · Ferropericlase · Force field simulations · Physical properties

Introduction

Minerals are thought of as long-range ordered crystalline materials, but solid solutions are common across many mineral classes, where the substitution of one ion for another introduces disorder, which can significantly influence physical properties such as density, optical behavior, magnetism, and electrical conductivity. Traditionally, such changes have been analyzed in terms of long-range structural motives, that influence properties like cleavage, stability, and elasticity (Putnis 1992). However, substitution of ions with different radii introduces local strain, and therefore locally influences the bonding environment. The possible effect of the explicit local distribution of ions that occupy the same site in the average crystallographic structure on material properties remains largely unexplored. A well-known example for a solid solution series is the forsterite–fayalite solid solution series, $(Fe_{xx}Mg_{1-x})_2SiO_4$ $(0<x<1)$, commonly referred to as olivine. As a dominant mineral in Earth's upper mantle, particularly near the forsterite endmember composition (e.g., $(Fe_{0.1}Mg_{0.9})_2SiO_4$) (McDonough and Rudnick 1998), olivine plays a critical role in controlling mantle rheology and seismic velocities. Olivine is abundant in mafic and ultramafic igneous rocks and various metamorphic settings. Beyond its geological importance, olivine and related phosphates with the olivine structure type have garnered interest for technological applications, including CO_2 sequestration through enhanced weathering (e.g., Montserrat et al. 2017; Fuhr et al. 2021), and as cathode materials in lithium-ion batteries (e.g., Heath et al. 2017).

The olivine structure (space group *Pnma*) contains two crystallographically distinct octahedral cation sites, M1 and M2, which are occupied by divalent Fe^{2+} and Mg^{2+}, while Si^{4+} occupies tetrahedral sites (see Fig. 1a. The M1 site shares edges with four neighboring octahedra (two M1 and two M2), forming chains along the *b*-axis. The M2 site shares edges with two M1 octahedra. Despite the similarity in the octahedral geometries, subtle differences in local bonding and crystallographic environment can lead

✉ Ella M. Schmidt
ella.schmidt@uni-bremen.de

[1] MARUM - Center for Marine Environmental Sciences, University of Bremen, 28359 Bremen, Germany

[2] Crystallography and Geomaterial Research, Faculty of Geosciences, University of Bremen, 28359 Bremen, Germany

[3] MAPEX Center for Materials and Processes, University of Bremen, 28359 Bremen, Germany

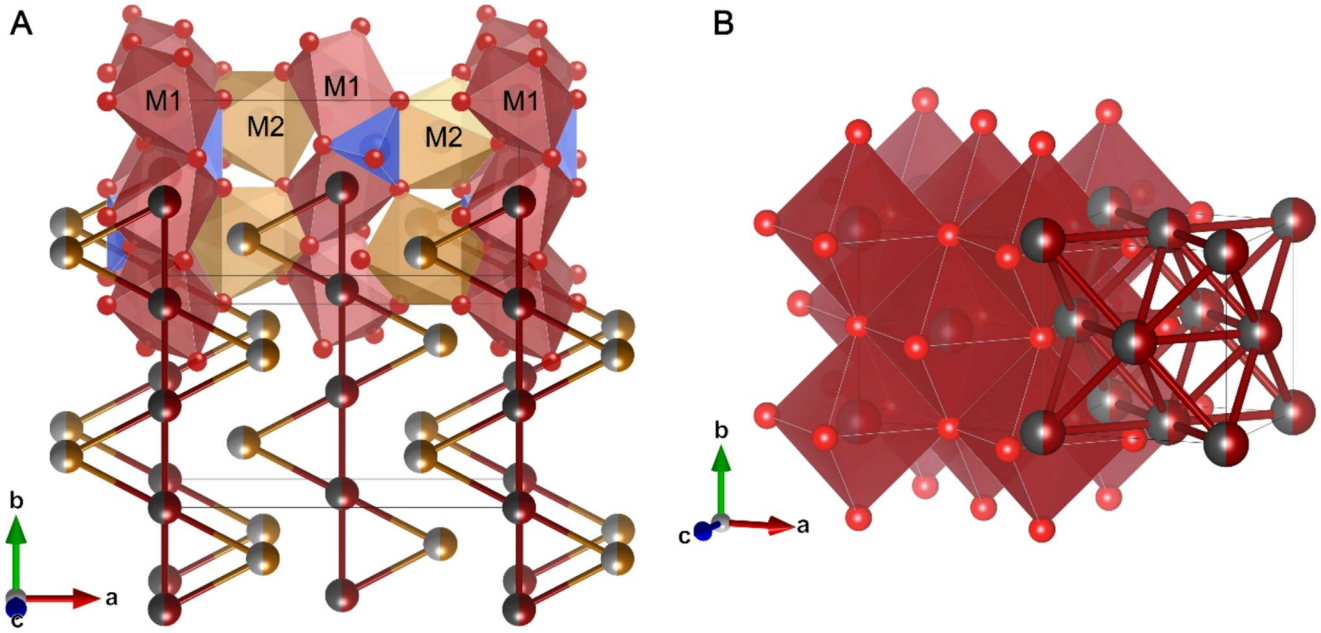

Fig. 1 **a** Average structure of the olivine solid solution in *Pnma* setting. The M1 site is shown in darker colors, while the M2 site is in lighter colors. Both sites contain equal amounts of Fe and Mg, represented by two-colored atoms (dark red and grey for M1 and light brown and grey for M2). Si in blue, O in red. Top: complete structural model, bottom: coarse grained description highlighting the chains of triangles along *b*, that are formed by edge-sharing octahedra. One single unit cell is indicated by the black box. **b** Average structure of ferropericlase solid solution ($Fm\bar{3}m$). Fe in dark red, Mg in dark gray, O in red. Left: complete structural model, right: coarse grained description highlighting the triangles of nearest neighbor cations. Figures generated with VESTA (Momma and Izumi 2011)

to preferential partitioning of cations between the M1 and M2 sites. In terms of the long-range average structure, various degrees of cation portioning have been observed in different olivine type structures (Müller-Sommer et al. 1997; Kądziołka-Gaweł et al. 2022; Jundullah Hanafi et al. 2024), while in LiMPO$_4$ olivines (M=Mn, Co, Fe, Ni), complete site partitioning has been reported (García-Moreno et al. 2001; Gnewuch and Rodriguez 2020).

In natural olivine, degrees of Fe^{2+}/Mg^{2+} partitioning vary and are intensively discussed in literature (Aikawa et al. 1985; Redfern et al. 2000; Morozov et al. 2005). Results from Artioli et al. (1995) and Rinaldi et al. (2000) show increasing preference for Fe^{2+} in M1 sites up to 900 °C, however at the same time an increase of Mg in M1 is observed between 900 °C and 1300 °C. Partially consistent results from e.g. Heinemann et al. (2007) and Morozov et al. (2005) show an increasing preference for Fe^{2+} in M1 at temperatures between 500 °C and 900 °C, but do not rule out a possible reversal of preferences at lower temperatures (300–350 °C). Opposite ordering behavior is proposed by Redfern et al. (2000), with a preference of Fe^{2+} in M2 sites at temperatures between 600 °C and 1250 °C. Only full cation partitioning refers to structures, that are accurately described by a long-range average structure. Local ordering, on the other hand, may occur even when no or only partial cation partitioning is present. A compositionally analogous but structurally much simpler solid solution is ferropericlase, $(Fe_{xx}Mg_{1-x})O$ $(0<x<1)$. Ferropericlase crystallizes in the rock salt (NaCl) structure and forms a complete solid solution between FeO and MgO. In this structure, Fe^{2+} and Mg^{2+} occupy a single symmetry-independent octahedral site (Fig. 1b), precluding long-range cation partitioning between distinct sites. However, local chemical ordering, deviations from a random distribution on this single site, is possible and has been reported in numerous rock salt-type compounds driven by short-range interactions (e.g., Billingham et al. 1972; Sauvage and Parthé 1972; Withers et al. 1994; Gusev 2006; Ji et al. 2019).

Local ordering can arise from various factors, including relatively weak chemical driving forces that are insufficient to establish long-range order (common in metastable phases formed at high temperatures) and geometric frustration, where the locally preferred atomic arrangement cannot be perfectly extended across the entire crystal lattice while maintaining the average structure (see Simonov and Goodwin 2020). Both the rock salt and olivine structures contain structural motifs prone to such frustration: face-sharing octahedra forming triangles of nearest-neighbor cations in ferropericlase, and edge-sharing octahedra forming triangular motifs in olivine (see Fig. 1).

Local ordering can manifest in two limiting scenarios: (1) Clustering of like cations (here Fe- or Mg-rich domains),

potentially leading to exsolution if sufficiently developed or (2) Anticlustering, or heteroatom paring as nearest neighbors, to better distribute strain from ionic size mismatches. In the first scenario, strain is concentrated at domain boundaries; in the second, it is more evenly distributed throughout the crystal.

Increasing evidence suggests that local chemical order significantly influences mechanical and physical properties in materials, particularly in alloys. For instance, short-range ordering has been harnessed to tailor mechanical behavior in alloys (e.g., Wu et al. 2021), where it has been shown that hardness, shear modulus and Youngs modulus can be tailored by local ordering (Narsu et al. 2013; Huang et al. 2018; Zhang et al. 2020).

Very few studies have explored the effects of local ordering on physical properties in important mineral structures that form solid solutions. In this study, we aim to contribute to filling this gap by explicitly investigating structures with identical long-range average structures, but variation in short-range ordering motives to determine their effect on physical properties. We employ computational modeling with empirical force fields to explore how different degrees of local cation ordering (clustering, random, anticlustering) influence the physical properties of olivine and ferropericlase solid solutions, focusing on compositions near $x \approx 0.5$. Specifically, we evaluate the effects on elastic properties (bulk and shear moduli), seismic wave velocities, heat capacities, and lattice dynamics (phonon dispersion). Some previous simulation studies did consider cation partitioning (Chatterjee et al. 2011) while to the best of our knowledge the possibility of local order has not been considered explicitly. Our aim is to quantify the significance of short-range ordering effects relative to compositional variations and assess their potential relevance for interpreting mineral behavior in geophysical and materials science contexts for these two important structural types.

Methods

Generation of supercells and ordering of cations

To investigate the influence of local cation ordering, we investigate composition of approximate 50:50 Mg:Fe, as here the most prominent effects are expected – even though these are not the most representative case for natural sample materials. For this purpose, we generated supercells encoding different degrees of local chemical order. For olivine, we created ten $10 \times 10 \times 2$ supercells based on the Mg_2SiO_4 olivine structure (Materials Project, Version 2021.11.10, entry mp-20313; Jain et al. 2013). This structure is given in the standard *Pnma* setting (space group 62), which we used throughout this study, rather than the commonly used *Pbnm* setting. The supercell size (5600 atoms each) was selected as a compromise between computational efficiency and physical accuracy. The implemented local ordering scheme includes nearest-neighbor octahedral pairs, which form chains in the *ab*-layer (see below). The resulting random order along *c*-axis results in negligible changes in calculated physical properties for longer supercells along the *c*-axis. In ferropericlase, nearest neighbors form a three-dimensional network, therefore we generated ten $10 \times 10 \times 10$ supercells (8000 atoms each) based on the MgO structure (Boiocchi et al. 2001) (ICSD-158106). Both sets of supercells started from pure Mg endmember structures, Mg_2SiO_4 for olivine and MgO for ferropericlase, and were converted to the final supercells used in the analysis via a two-step process.

Local chemical ordering was introduced using the program DISCUS (Proffen and Neder 1997). Starting with the pure Mg supercells, Mg atoms were randomly substituted by Fe to achieve an approximate 50:50 composition. Subsequently, a Monte Carlo simulation swaps Fe and Mg atoms on the same average structure site to achieve a specific target value of the Warren–Cowley short-range order (SRO) parameter, α (Warren et al. 1951). The parameter α is defined as:

$$\alpha = 1 - \frac{p_{MgFe}}{m_{Mg} m_{Fe}} \quad (1)$$

p_{MgFe} represents the probability of finding Mg–Fe (or Fe–Mg) pairs on nearest neighbor cation sites, and m_{Mg} and m_{Fe} are the molar fractions of Mg and Fe, respectively. This definition allows for the representation of three limiting ordering types: $\alpha > 0$ corresponds to preferential clustering of like cations (more Mg–Mg and Fe–Fe pairs); $\alpha \approx 0$ represents an essentially random distribution; and $\alpha < 0$ indicates preferential anticlustering (more Mg–Fe and Fe–Mg pairs). It should be noted that by applying this methodology, all investigated structures are identical in terms of the average structure (including all site-occupancies and the absence of cation-partitioning) and only show variations in the local ordering.

In the olivine structure, nearest-neighbor cation interactions occur between edge-sharing octahedra. The M1 site has four nearest cation neighbors (two M1, two M2), while the M2 site has two nearest cation neighbors (both M1). Due to the specific topology of the octahedral network and geometric frustration, perfect anticlustering ($\alpha = -1$) is not possible; the maximum attainable α for anticlustered structures is approximately -0.33. Clustering simulations yielded α values up to 0.84. In the ferropericlase structure, each cation has 12 nearest cation neighbors. This higher coordination and network topology also introduces geometric frustration,

Table 1 Achieved Warren-Cowley short range order parameters a in the investigated supercells for the three cases of local ordering: Anticlustering, clustering and random distribution.

	Olivine			Ferropericlase		
	min	max	average	min	max	average
Anticluster	-0.339	-0.333	-0.335	-0.289	-0.267	-0.281
Cluster	0.825	0.868	0.844	0.802	0.832	0.814
Random	-0.027	0.046	0.001	-0.050	0.067	-0.008

Table 2 Parameters from Quarderny et al. (2015) for the empirical pair Potentials. C as reported in Pedone et al. (2006)

Pair	D (eV)	a ($Å^{-1}$)	r_0 (Å)	C (eV $Å^{12}$)
Mg – O	0.123583	2.045583	2.424824	5.0
Fe – O	0.064948	1.888936	2.644110	2.0
Si – O	0.443427	1.758024	2.081625	1.0
O – O	0.042323	1.311417	3.762599	22.0

limiting the achievable SRO values to approximately -0.28 for anticlustering and 0.81 for clustering. Table 1 summarizes the range and average SRO values achieved for the generated supercells across the three ordering types.

Structural relaxation of supercells and calculation of physical properties

Structural relaxation of all generated supercells was performed using classical interatomic potentials as implemented in the General Utility Lattice Program (GULP) (Gale 2005). Calculations were conducted under constant pressure and temperature conditions (1 atm, 298 K), without constraints on the unit cell parameters. All symmetry constraints were removed to appropriately treat the disordered nature of the supercells.

Two empirical interatomic potential models were evaluated for structure optimization: a Buckingham potential with additional three-body and spring terms (Walker et al. 2003) and a combination of Morse and Lennard-Jones pair potentials (Quadery et al. 2015). Elastic constants derived from the second potential model were reported to be closer to experimental values for the Mg endmember of olivine (Pedone et al. 2006) (see Supplementary Information Table S1 for comparison), and this model was therefore used for all subsequent relaxations and property calculations presented in this study. The parameters for the chosen potential model are listed in Table 2.

Physical properties, including elastic moduli (bulk, shear, Young's), Poisson's ratio, and seismic wave velocities (compressional v_p and shear v_s), were computed from the relaxed supercell structures using standard methods implemented in GULP (derived from the elastic constant tensor).

Heat capacity at constant volume (C_v) was calculated from the vibrational density of states obtained from phonon calculations (described below). Structural relaxation and property calculations were conducted using the serial GULP implementation. Phonon calculations were performed using GULP's parallel implementation to improve computational efficiency.

Phonon calculations were performed using the supercell lattice dynamical (SCLD) method (Overy et al. 2016, 2017; Schmidt et al. 2022; Roth and Goodwin 2023). Conventional lattice dynamics samples the dynamical matrix $\boldsymbol{D}\left(\vec{k}\right)$ at a suitably dense set of wave-vectors $\vec{k}$ in the primitive cell's Brillouin zone. This is appropriate for perfectly periodic crystals. However, for disordered structures simulated within a supercell, the disorder configuration breaks the translational symmetry of the average structure. SCLD addresses this by performing lattice dynamics calculations for the supercell, where the dynamical matrix is typically sampled only at the supercell's Γ-point ($\vec{k} = (000)$). Band undfolding then allows to probe the resulting phonon frequencies that correspond to wavevectors in the primitive cell Brillouin zone that are commensurate with the supercell size:

$$\vec{k} = \left(\frac{n_a}{N_a}, \frac{n_c}{N_b}, \frac{n_c}{N_c}\right); \quad n_i \in \{0,1,\ldots N_i - 1\}, \tag{2}$$

where N_a, N_b and N_c describe the size of the supercell along the *a*-, *b*- and *c*-direction respectively.

The phonon eigenvalues and eigenvectors were calculated using GULP, while the band unfolding was performed by a custom Fortran code. The SCLD method, as employed here following previous studies on disordered systems (Overy et al. 2016; Schmidt et al. 2022; Roth and Goodwin 2023), is well-suited for analyzing the vibrational properties of explicitly disordered supercells.

Results

Physical properties of the olivine solid solution

The computed bulk physical properties for the olivine supercells, including bulk modulus (K), compressional velocity (v_p) and Poisson's ratio (ν), are presented in Fig. 2. Further properties, such as shear modulus (G), shear velocity (v_s) and Young's modulus (E) along with the computed entropy are shown in the Supplementary Information Fig.

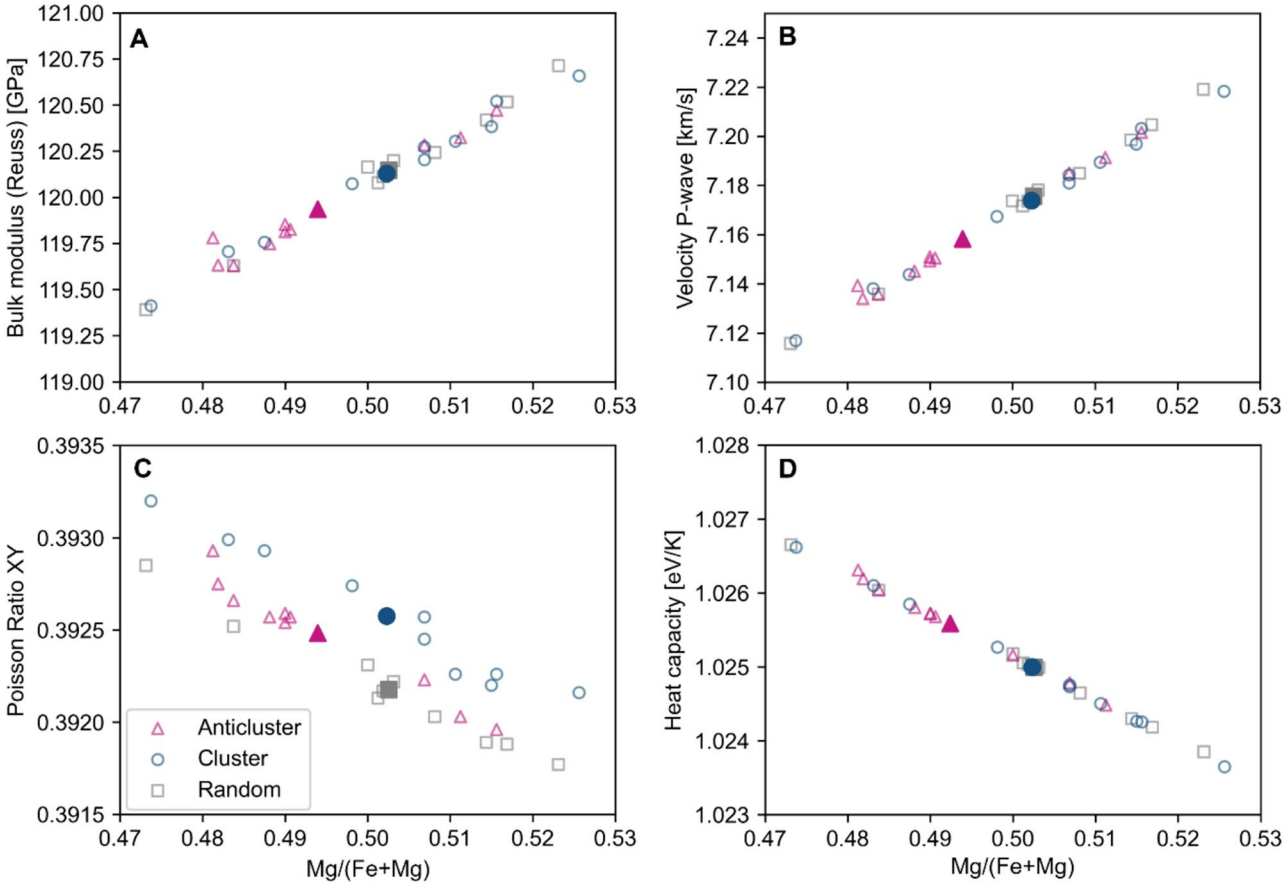

Fig. 2 Selected physical properties of the olivine solid solution series as calculated from disordered supercells using GULP. Structures with anticlustering ($\alpha \approx -0.335$) are shown as pink triangles, structures with clustering ($\alpha \approx +0.848$) of likewise atoms are shown as blue circles, randomly ordered structures ($\alpha \approx 0$) are shown as gray squares. Filled in symbols show the average over the respective short-range order type.

S2. The computed entropy varies negligibly among the tested configurations. This indicates that the structures can effectively compensate for the strain that arise from different local cation orderings. For the majority of the computed physical properties, compositional variations among the ten generated supercells for each ordering type exert a significantly larger influence than the degree of local cation ordering (clustering vs. random vs. anticlustering). The spread in values for each ordering type is primarily due to slight deviations from the target 50:50 composition in the generated supercells, highlighting the strong compositional control.

A minor systematic trend related to short-range order is observed for the Poisson ratio, particularly in the plane perpendicular to the *c*-axis (*xy*-direction), where structures exhibiting clustering show a slight increase compared to random or anticlustered configurations (Fig. 2C). This subtle trend is also reflected in the Young's modulus along the *y*-direction (see Supplementary Information Fig. S2). These observations may be related to the arrangement of the triangular-linked chains of nearest-neighbor cations along the *b*-direction (Fig. 1a). Overall, the variations in bulk physical properties directly attributable to differences in short-range order are small, often falling within the typical uncertainties of experimental measurements or the inherent discrepancies between empirical force field simulations and experimental data.

Phonon dispersion of the olivine solid solution

To assess the influence of local ordering on the lattice dynamics, phonon dispersion curves were derived from band-unfolded SCLD simulations for representative supercells with different degrees of cation order (Fig. 3). The phonon dispersion curves for anticlustered and randomly ordered structures are nearly indistinguishable. In contrast, clustered structures display slightly sharper and more defined band structures, particularly at higher frequencies (200–300 cm^{-1}) along certain directions in reciprocal space (e.g., between the S and Y points). The differential phonon dispersion curve between clustered and anticlustered structures

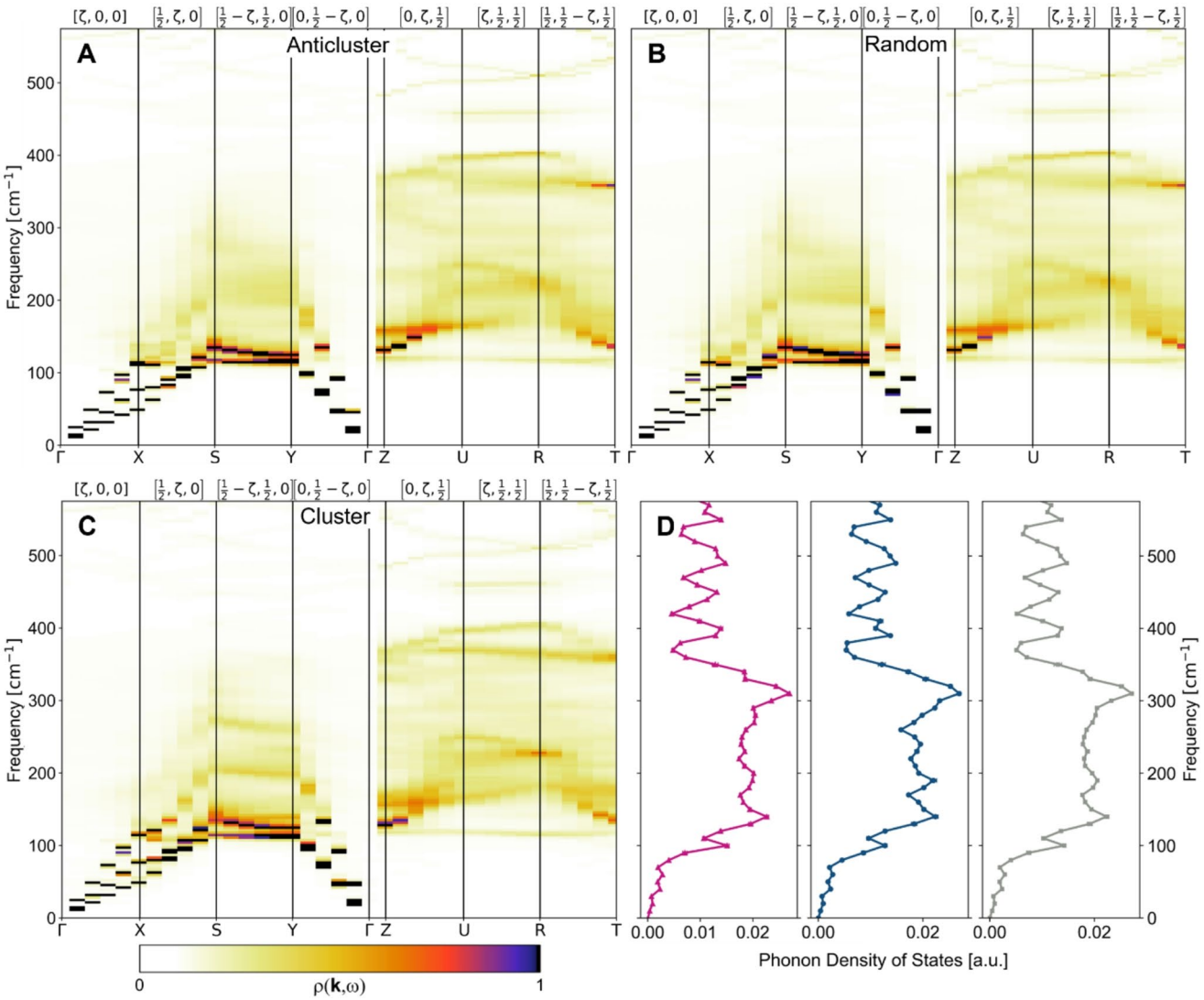

Fig. 3 Phonon Dispersion of the middle member of the olivine solid solution series with the effect of different short-range order parameters. Band unfold SCLD projection ρ(**k**, w) along key directions in reciprocal space. **A** Anticlustering ($\alpha \approx -0.335$);**B** random ordering ($\alpha \approx 0$); **C** clustering ($\alpha \approx +0.848$). **D** shows the phonon density of states for the three different ordering types: anticlustering in pink, clustering in blue and random order in gray.

further highlights these subtle distinctions (see Supplementary Information Fig. S3). Despite these small variations in the dispersion curves, the calculated total phonon densities of states for the three ordering types are remarkably similar, showing negligible differences (Fig. 3D).

Physical properties of the ferropericlase solid solution

In contrast to olivine, ferropericlase shows more noticeable systematic variations in some bulk physical properties depending on the degree of local cation ordering (Fig. 4). Structures exhibiting clustering generally show lower values of bulk modulus (K), shear modulus (G), and consequently, lower seismic wave velocities (v_p and v_s) compared to anticlustered counterparts (Fig. 4 and Supplementary Information Fig. S5). Randomly ordered structures typically show values close to the anticlustered structures. This is also in agreement with the observed differences in the configurational entropy shown in the Supporting Information (Fig. S5).

The Poisson ratio (Fig. 4C) remains relatively stable across different ordering states in ferropericlase, showing even less variations than in the olivine solid solution. The heat capacity (C_v, Fig. 4D) shows the most pronounced sensitivity to local ordering among the calculated bulk properties, with a clear separation between clustered (lowest C_v), anticlustered (highest C_v), and random disorder (intermediate C_v). As in the olivine system, compositional variations within the sampled supercells still exert a significant

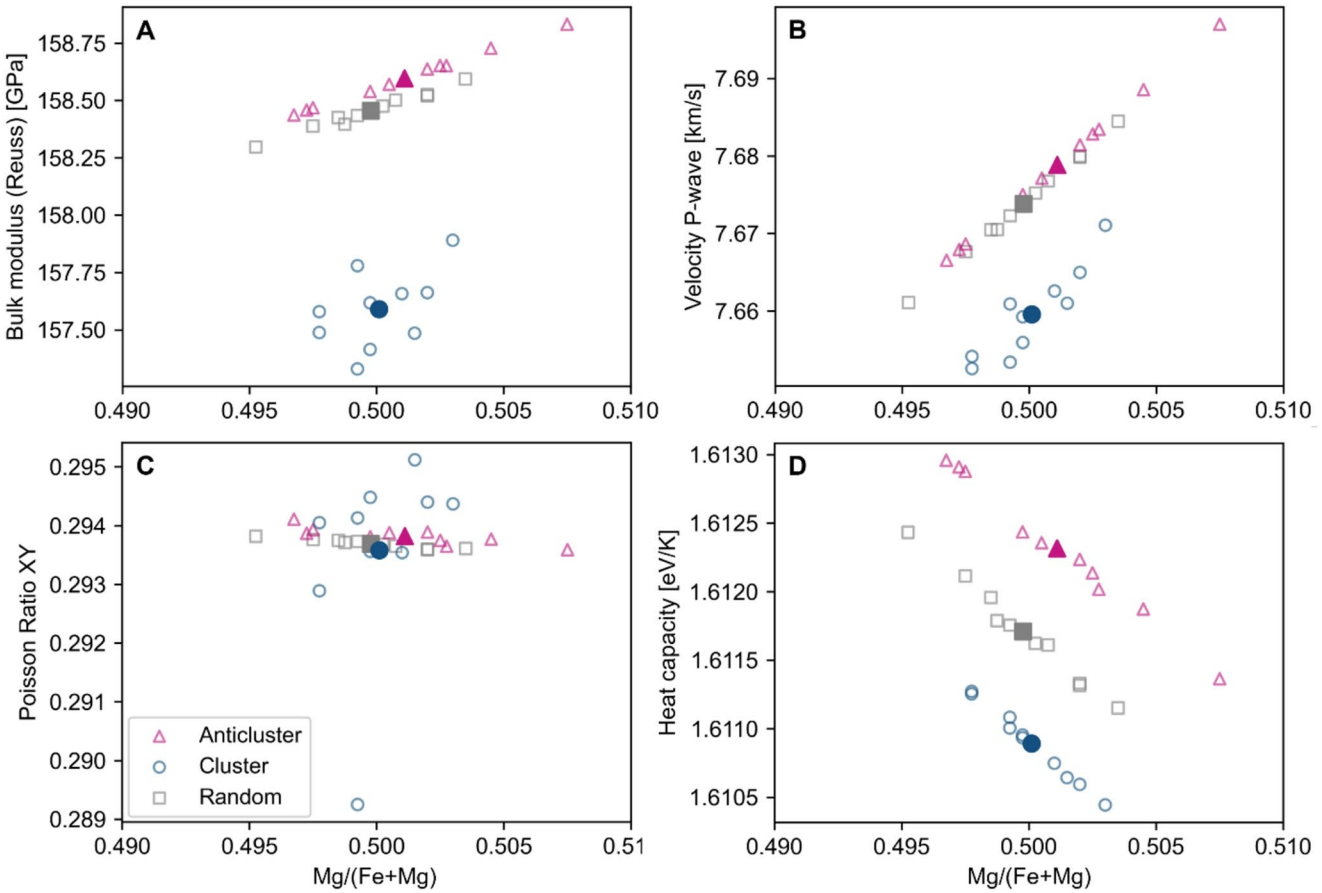

Fig. 4 Selected physical properties of the ferropericlase solid solution series as calculated from disordered supercells using GULP. Structures with anticlustering ($\alpha \approx -0.281$) are shown as pink triangles, structures with clustering ($\alpha \approx +0.814$) of likewise atoms are shown as blue circles, randomly ordered structures ($\alpha \approx 0$) are shown as gray squares. Filled in symbols show the average over the respective short-range order type.

influence on most properties, but the effect of clustering in making the structure "softer" (lower elastic moduli) is more evident in ferropericlase.

Phonon dispersion of the ferropericlase solid solution

Phonon dispersion curves calculated along key reciprocal-space directions reveal more distinct effects of local ordering in ferropericlase compared to olivine (Fig. 5). Between the Γ and X points, two narrow, low-frequency acoustic-like bands are visible in clustered structures. In anticlustered structures, only one such band appears, while randomly ordered systems exhibit substantial phonon-band broadening, effectively merging multiple bands. Clustered structures generally display sharper and more defined phonon bands across the spectrum, suggesting that the vibrations resemble those of distinct Mg-rich and Fe-rich regions. In contrast, anticlustered and especially random structures show increasing degrees of band broadening, indicative of increased phonon scattering due to structural disorder. Between the X and X′ points, both random and anticlustered structures show a clearer separation or band gap between acoustic and optical branches, which is less pronounced or absent in clustered structures where the optical and acoustic bands converge. Furthermore, the total phonon density of states (DoS) shows more pronounced differences among the ordering types compared to olivine (compare Fig. 3d to Fig. 5d). Notably, the DoS for clustered ferropericlase shows a significant maximum at around 220 cm^{-1}, which is absent in the anticlustered and randomly sorted structures.

Discussion

This study investigated the middle members (near $x=0.5$) of the olivine and ferropericlase solid solution series across three distinct states of local cation ordering: clustering, random distribution, and anticlustering. By using atomistic simulations with explicit arrangements of cations in supercells,

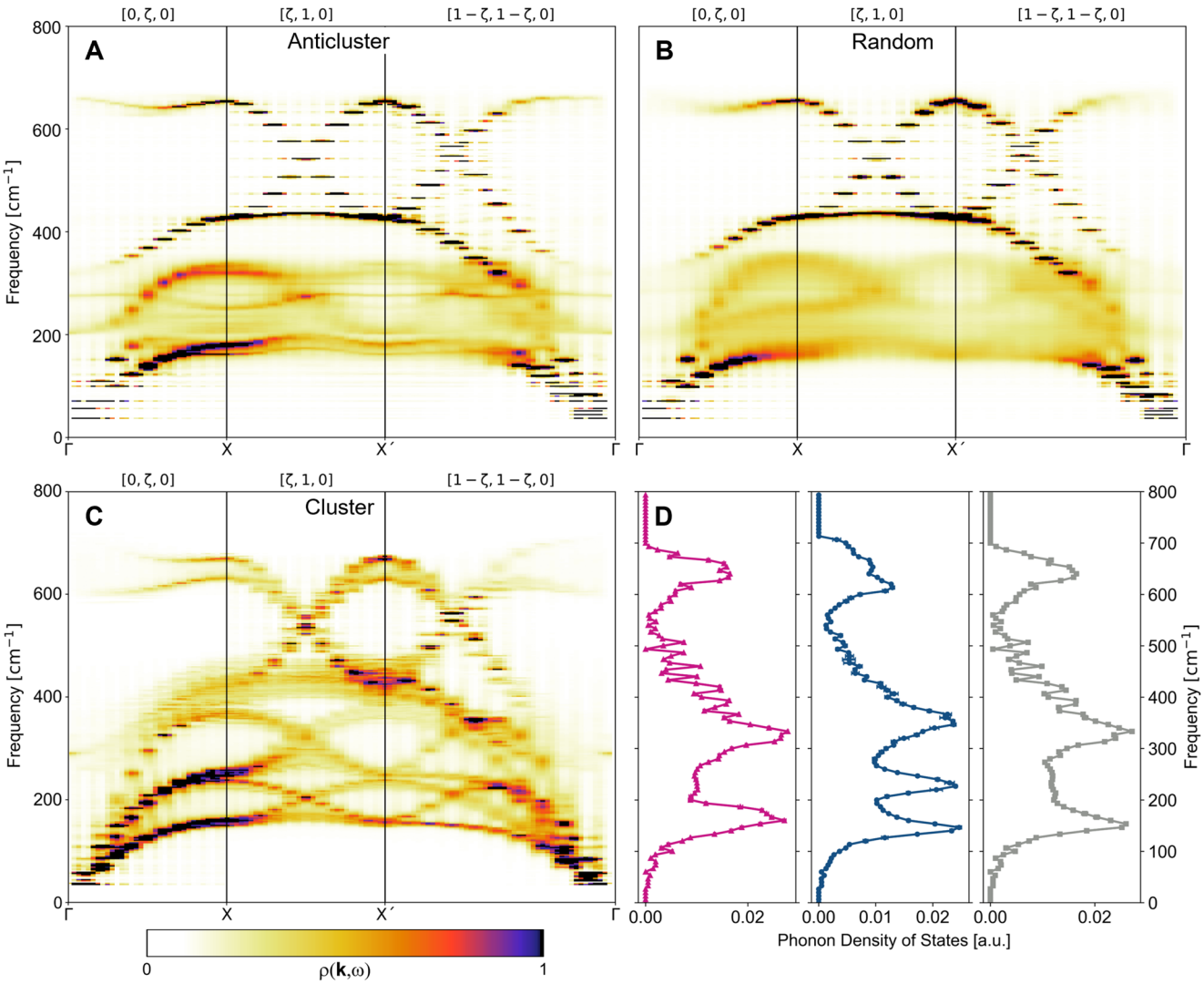

Fig. 5 Phonon Dispersion of the middle member of the ferropericlase solid solution series with the effect of different short-range order parameters. Band unfold SCLD projection ρ(**k**, w) along key directions in reciprocal space. **A** Anticlustering ($\alpha \approx -0.281$); **B** random order ($\alpha \approx 0$); **C** clustering ($\alpha \approx +0.814$) **D** shows the phonon density of states for the three different ordering types: anticlustering in pink, clustering in blue and random order in gray.

we disentangle the influence of local structural organization from the fundamental differences in mass and ionic size between Mg and Fe that define the overall composition.

A primary finding across both mineral systems is that overall chemical composition (specifically, minor variations in the Fe/Mg ratio within the nominally 50:50 samples) has a more pronounced effect on the values of most bulk physical properties compared to the influence of short-range cation order. This is consistent with the fact that bulk elastic properties, derived from the second derivatives of the potential energy with respect to strain, reflect the overall stiffness and bond strengths within the material. For the olivine system, the simulated structures show no significant variations in the configurational entropy (see Supporting Information Fig. S2) that depend on the local ordering. Therefore, variations in the total bond energy of the system due to the substitution of Mg–O bonds with weaker Fe–O bonds (as parameterized in the force field, Quarderny et al.2015) naturally lead to systematic changes in elastic moduli and seismic velocities as composition varies. Increased Mg content results in generally stiffer structures with higher moduli and faster seismic wave velocities. While expected, this compositional control serves as an important baseline against which the subtler effects of local ordering must be compared. In ferropericlase, our results show that configurations with cation clustering exhibit higher configurational entropy than those with anticlustering or random ordering (see Supporting Information, Fig. S5). We attribute this to the formation of distinct Fe-rich and Mg-rich domains, which likely introduces strain at the domain boundaries due to imperfect

accommodation of preferred bonding arrangements. This reduced structural stability is reflected in the bulk physical properties, leading to a lower bulk modulus and P-wave velocity for the clustered configurations.

While we observe these subtle effects, our simulations demonstrate that composition is the dominant factor controlling the bulk properties of both ferropericlase and olivine. This finding provides an important contrast to other material classes, such as complex alloys, where local ordering is increasingly recognized as a primary mechanism for tuning physical and mechanical properties (e.g., Wu et al. 2021). The extent to which these principles from materials science apply to structurally more complex mantle minerals is explored in our study. For the structurally very simple solid solution ferropericlase and structurally medium complex solid solution olivine, the influence of local ordering on physical properties such as elasticity is secondary to the overall cation ratio. This suggests that concepts on altering local ordering from alloy design may not be directly transferable to these more complex mineral systems and hence the influence on bulk properties is minor.

The phonon dispersion curves and densities of states, derived from the SCLD calculations, directly probe how the local bonding environments affect the collective atomic motions in the form of phonons. Our results reveal a striking contrast in the sensitivity of vibrational properties to local ordering between ferropericlase and olivine. The simpler rock salt structure of ferropericlase, with its high coordination number and direct face-sharing linkage between neighboring octahedra, shows pronounced variations in phonon dispersion and density of states depending on the SRO type. Cation clustering leads to band splitting reminiscent of mixing the phonon spectra of the pure endmembers (MgO and FeO), as observed previously in other rock salt solid solutions like KCl_xBr_{1-x} (Schmidt et al. 2022). Anticlustering tends to produce phonon features closer to those predicted by the virtual crystal approximation (VCA), which assumes an average atom. Random ordering results in significant phonon band broadening due to scattering from disorder. These distinct changes in the phonon DoS directly explain the observed variations in calculated heat capacity (C_v) for ferropericlase (Fig. 4d), as C_v is directly derived from the DoS. Notably, here we also observe variations between the random and anti-clustered ordering, suggesting that these vibrational properties are not only influenced by the differences in the configurational entropy.

As compared to ferropericlase, the olivine solid solution exhibits much subtler changes in its phonon dispersion and a negligible difference in the total phonon DoS across different ordering states (Fig. 3d). This reduced sensitivity is likely attributable to the increased structural complexity and bonding topology of olivine compared to ferropericlase. The olivine structure contains a larger number of atoms per unit cell (28 atoms in the primitive cell, leading to 84 distinct vibrational modes), resulting in a much denser and more complex phononic band structure (Price et al. 1987). In this densely populated spectrum, the relatively small variations introduced by local Fe-Mg disorder appear smeared out or masked by the multitude of overlapping modes. Furthermore, the presence of relatively rigid SiO_4 tetrahedra within the olivine structure may buffer the overall vibrational dynamics against local variations in cation ordering, limiting the extent to which different Mg-Fe arrangements can perturb the high-frequency internal modes of the tetrahedra or the lower-frequency external modes involving coupled cation and tetrahedral movements.

Conclusion

This study demonstrates that while overall compositional variations exert the dominant control on the bulk physical properties of (Fe, Mg) solid solutions, local short-range cation ordering can still exert a notable influence, particularly on vibrational dynamics. Using force field simulations of explicitly ordered supercells of olivine and ferropericlase (near $Fe_{0.5}Mg_{0.5}$), we compared the effects of clustering, random distribution, and anticlustering.

Of the two systems we investigated olivine is the structurally more complex mineral, where the effects of short-range order on phonon dispersion and bulk physical properties are minimal compared to compositional effects. This is likely due to the intricate connectivity of rigid SiO_4 tetrahedra and the resulting dense phononic band structure, which tends to mask subtle differences introduced by local cation arrangements. In contrast, the simpler rock salt structure of ferropericlase, with its higher cation coordination and less constrained bonding network, exhibits clearer variations in both phonon dispersion and density of states directly tied to local ordering. We believe our observations can be transferred to other simple structures with robust ionic bonds, while framework structures such as zeolites where effects such as ridged unit modes (Hammonds et al. 1996) play a role would require a more explicit investigation.

Changes in the vibrational landscape due to local ordering as we observe here can potentially influence a range of thermophysical properties, including soft phonon modes, which are relevant for understanding structural instabilities or phase transitions, thermal conductivity (κ), which depends on phonon group velocities, scattering rates, and lifetimes as well as ion migration pathways, potentially affecting diffusion and electrical conductivity, as these are shaped by the local energy landscape and atomic vibrations. These vibrational characteristics furthermore directly

impact thermoelastic properties, such as volume thermal expansion, which are essential input parameters for geophysical models of Earth's interior.

Overall, while compositional effects are paramount for many bulk properties of mineral solid solutions, local ordering is not negligible. Its impact on lattice dynamics, particularly in simpler structures, highlights the importance of considering short-range order when interpreting derived thermodynamic properties and linking atomic-scale structure to macroscopic geophysical behavior. To transfer our findings to real-world scenarios, variable temperature and pressure conditions need to be taken into account, as pressure affects bond strengths and therefore can alter the dependence of the observed properties on local order. These effects offer an interesting avenue of further research.

Supplementary Information The online version contains supplementary material available at https://doi.org/10.1007/s00269-025-01333-9.

Acknowledgements C.W. acknowledges support by the MARUM Research Academy, University of Bremen. Paul Benjamin Klar, Christoph Vogt and Wolfgang Bach (all University of Bremen) are acknowledged for fruitful discussions.

Author contributions C.W. performed the simulations, curated and interpreted the data, and prepared all figures.E.M.S. supervised the project and assisted with data curation and interpretation.C.W. and E.M.S. jointly wrote the main manuscript.

Funding Open Access funding enabled and organized by Projekt DEAL.

Data availability No datasets were generated or analysed during the current study.

Declarations

Conflict of interest The authors declare no competing interests.

References

Aikawa N, Kumazawa M, Tokonami M (1985) Temperature dependence of intersite distribution of Mg and Fe in olivine and the associated change of lattice parameters. Phys Chem Minerals 12:1–8. https://doi.org/10.1007/BF00348738

Artioli G, Rinaldi R, Wilson CC, Zanazzi PF (1995) High-temperature Fe-Mg cation partitioning in olivine; in-situ single-crystal neutron diffraction study. Am Mineral 80:197–200. https://doi.org/10.2138/am-1995-1-223

Billingham J, Bell PS, Lewis MH (1972) Vacancy short-range order in substoichiometric transition metal carbides and nitrides with the NaCl structure. I. Electron diffraction studies of short-range ordered compounds. Acta Cryst A 28:602–606. https://doi.org/10.1107/S0567739472001524

Boiocchi M, Caucia F, Merli M et al (2001) Crystal-chemical reasons for the immiscibility of periclase and wustite under lithospheric P,T conditions. Ejm 13:871–881. https://doi.org/10.1127/0935-1221/2001/0013/0871

Chatterjee S, Bhattacharyya S, Sengupta S, Saha-Dasgupta T (2011) Crossover of cation partitioning in olivines: a combination of Ab initio and Monte Carlo study. Phys Chem Miner 38:259–265

Fuhr M, Geilert S, Schmidt M, Wallmann K (2021) Kinetics of olivine weathering in seawater: an experimental study. Goldschmidt2021 abstracts. European Association of Geochemistry, Virtual

Gale JD (2005) GULP: capabilities and prospects. Z für Kristallographie - Crystalline Mater 220:552–554. https://doi.org/10.1524/zkri.220.5.552.65070

García-Moreno O, Alvarez-Vega M, García-Alvarado F et al (2001) Influence of the structure on the electrochemical performance of lithium transition metal phosphates as cathodic materials in rechargeable lithium batteries: A new High-Pressure form of $LiMPO_4$ (M = Fe and Ni). Chem Mater 13:1570–1576. https://doi.org/10.1021/cm000596p

Gnewuch S, Rodriguez EE (2020) Distinguishing the intrinsic antiferromagnetism in polycrystalline $LiCoPO_4$ and $LiMnPO_4$ olivines. Inorg Chem 59:5883–5895. https://doi.org/10.1021/acs.inorgchem.9b03545

Gusev AI (2006) Short'range order and diffuse scattering in nonstoichiometric compounds. Uspekhi Fizicheskikh Nauk 176:717. https://doi.org/10.3367/UFNr.0176.200607b.0717

Hammonds KD, Dove MT, Giddy AP *et al* (1996) Rigid-unit modes and structural phase transitions in framework silicates. American Mineralogist 81:1057-1079 https://doi.org/10.2138/am-1996-9-1003

Heath J, Chen H, Islam MS (2017) $MgFeSiO_4$ as a potential cathode material for magnesium batteries: ion diffusion rates and voltage trends. J Mater Chem A 5:13161–13167. https://doi.org/10.1039/C7TA03201C

Heinemann R, Kroll H, Kirfel A, Barbier B (2007) Order and antiorder in olivine III: variation of the cation distribution in the Fe,Mg olivine solid solution series with temperature and composition. Ejm 19:15–27. https://doi.org/10.1127/0935-1221/2007/0019-0015

Huang S, Li W, Holmström E, Vitos L (2018) Strengthening induced by magnetochemical transition in al -Doped Fe - Cr - Co - Ni High-Entropy alloys. Phys Rev Appl 10:064033. https://doi.org/10.1103/PhysRevApplied.10.064033

Jain A, Ong SP, Hautier G et al (2013) Commentary: the materials project: A materials genome approach to accelerating materials innovation. APL Mater 1:011002. https://doi.org/10.1063/1.4812323

Ji H, Urban A, Kitchaev DA et al (2019) Hidden structural and chemical order controls lithium transport in cation-disordered oxides for rechargeable batteries. Nat Commun 10:592. https://doi.org/10.1038/s41467-019-08490-w

Jundullah Hanafi MI, Mursheda MM, Robben L, Gesing TM (2024) Mechanochemical synthesis of $(Mg_{1-x}Fe_x)_2SiO_4$ olivine phases relevant to Martian regolith: structural and spectroscopic

characterizations. Z für Kristallographie - Crystalline Mater 239:261–271. https://doi.org/10.1515/zkri-2024-0078

Kądziołka-Gaweł M, Wojtyniak M, Klimontko J (2022) High temperature transformation of iron-bearing minerals in basalt: Mössbauer spectroscopy studies. Mineralogia 53:10–19. https://doi.org/10.2478/mipo-2022-0002

McDonough WF, Rudnick RL (1998) Chap. 4. MINERALOGY AND COMPOSITION OF THE UPPER MANTLE. In: Hemley RJ (ed) Ultrahigh Pressure Mineralogy. De Gruyter, pp 139–164

Momma K, Izumi F (2011) *VESTA 3* for three-dimensional visualization of crystal, volumetric and morphology data. J Appl Crystallogr 44:1272–1276. https://doi.org/10.1107/S0021889811038970

Montserrat F, Renforth P, Hartmann J et al (2017) Olivine dissolution in seawater: implications for CO_2 sequestration through enhanced weathering in coastal environments. Environ Sci Technol 51:3960–3972. https://doi.org/10.1021/acs.est.6b05942

Morozov M, Brinkmann C, Lottermoser W et al (2005) Octahedral cation partitioning in Mg,Fe2+-olivine. Mossbauer spectroscopic study of synthetic (Mg0.5 Fe2+0.5)2SiO4(Fa50). Ejm 17:495–500. https://doi.org/10.1127/0935-1221/2005/0017-0495

Müller-Sommer M, Hock R, Kirfel A (1997) Rietveld refinement study of the cation distribution in (Co, Mg)-olivine solid solution. Phys Chem Miner 24:17–23. https://doi.org/10.1007/s002690050013

Narsu B, Wang G-S, Johansson B, Vitos L (2013) Large magneto-chemical-elastic coupling in highly magnetostrictive Fe-Ga alloys. Appl Phys Lett 103:231903. https://doi.org/10.1063/1.4838657

Overy AR, Cairns AB, Cliffe MJ et al (2016) Design of crystal-like aperiodic solids with selective disorder–phonon coupling. Nat Commun 7:10445. https://doi.org/10.1038/ncomms10445

Overy AR, Simonov A, Chater PA et al (2017) Phonon broadening from supercell lattice dynamics: random and correlated disorder. Phys Status Solidi (b) 254:1600586

Pedone A, Malavasi G, Menziani MC et al (2006) A new Self-Consistent empirical interatomic potential model for Oxides, Silicates, and Silica-Based glasses. J Phys Chem B 110:11780–11795. https://doi.org/10.1021/jp0611018

Price GD, Parker SC, Leslie M (1987) The lattice dynamics and thermodynamics of the Mg2SiO4 polymorphs. Phys Chem Minerals 15:181–190. https://doi.org/10.1007/BF00308782

Proffen Th, Neder RB (1997) *DISCUS*: a program for diffuse scattering and defect-structure simulation. J Appl Crystallogr 30:171–175. https://doi.org/10.1107/S002188989600934X

Putnis A (1992) An introduction to mineral sciences. Cambridge University Press

Quadery AH, Pacheco S, Au A et al (2015) Atomic-scale simulation of space weathering in olivine and orthopyroxene. JGR Planet 120:643–661. https://doi.org/10.1002/2014JE004683

Redfern SAT, Artioli G, Rinaldi R et al (2000) Octahedral cation ordering in olivine at high temperature. II: an in situ neutron powder diffraction study on synthetic MgFeSiO 4 (Fa50). Phys Chem Miner 27:630–637. https://doi.org/10.1007/s002690000109

Rinaldi R, Artioli G, Wilson CC, McIntyre G (2000) Octahedral cation ordering in olivine at high temperature. I: in situ neutron single-crystal diffraction studies on natural mantle olivines (Fa12 and Fa10). Phys Chem Miner 27:623–629. https://doi.org/10.1007/s002690000110

Roth N, Goodwin AL (2023) Tuning electronic and phononic States with hidden order in disordered crystals. Nat Commun 14:4328. https://doi.org/10.1038/s41467-023-40063-w

Sauvage M, Parthé E (1972) Vacancy short-range order in substoichiometric transition metal carbides and nitrides with the NaCl structure. II. Numerical calculation of vacancy arrangement. Acta Cryst A 28:607–616. https://doi.org/10.1107/S0567739472001536

Schmidt EM, Thomas S, Bulled JM et al (2022) Interplay of thermal diffuse scattering and correlated compositional disorder in $KCl_{1-x}Br_x$. Acta Crystallogr B Struct Sci Cryst Eng Mater 78:385–391. https://doi.org/10.1107/S2052520622003560

Simonov A, Goodwin AL (2020) Designing disorder into crystalline materials. Nat Rev Chem 4:657–673. https://doi.org/10.1038/s41570-020-00228-3

Walker AM, Wright K, Slater B (2003) A computational study of oxygen diffusion in olivine. Phys Chem Miner 30:536–545. https://doi.org/10.1007/s00269-003-0358-7

Warren BE, Averbach BL, Roberts BW (1951) Atomic size effect in the X-Ray scattering by alloys. J Appl Phys 22:1493–1496. https://doi.org/10.1063/1.1699898

Withers RL, Otero-Diaz LC, Thompson JG (1994) A TEM study of defect ordering in a calcium yttrium sulfide solid solution with an average NaCl-Type structure. J Solid State Chem 111:283–293. https://doi.org/10.1006/jssc.1994.1229

Wu Y, Zhang F, Yuan X et al (2021) Short-range ordering and its effects on mechanical properties of high-entropy alloys. J Mater Sci Technol 62:214–220. https://doi.org/10.1016/j.jmst.2020.06.018

Zhang R, Zhao S, Ding J et al (2020) Short-range order and its impact on the crconi medium-entropy alloy. Nature 581:283–287. https://doi.org/10.1038/s41586-020-2275-z